# Supporting Information

# A Dual-Mode Aptasensor Integrating Ratiometric Fluorescence and Colorimetry for On-Site $Cu^{2+}$ Detection

Lingli Bu,[a] Xia Yang,[a] Shenao Qu,[a] Junhao Hu,[a] Qingwei Cui,[e] Mengqi Wang,[e] Yue Wang,*[a] Kai Shi,*[c] Sheng Lei,*[d] Jiaheng Zhang*[b]

[a] Henan Linker Technology Key Laboratory, College of Advanced Interdisciplinary Science and Technology (CAIST), Henan University of Technology, Zhengzhou 450001, China. E-mail: wangyue@haut.edu.cn

[b] College of Chemistry, Zhengzhou University, Zhengzhou, 450001, PR China. E-mail: zhangjiaheng@zzu.edu.cn

[c] College of New Energy Materials and Chemistry, Leshan Normal University, Leshan Sichuan 614000, P. R. China. E-mail: shikai9901@163.com

[d] Department of Clinical Laboratory, The First Affiliated Hospital of Guangzhou Medical University, Guangzhou Medical University, Guangzhou, Guangdong, China. E-mail: smellred@163.com

[e] Henan Institute of Special Equipment Inspection Technology, Zhengzhou 450000, China.

# 1. Materials and Instruments

## 1.1 Chemicals and Materials

All chemicals used were of analytical grade or higher. Commercial coumarin dyes and various metal salts, including $FeSO_4 \cdot 7H_2O$, $FeCl_3 \cdot 6H_2O$, $PdCl_2$, $CrCl_3$, $NiCl_2$, $PbCl_2$, CuI, $ZnI_2$, $CoF_2$, $CaCl_2$, $MnSO_4$, $BaCl_2$, $ZrCl_4$, $CdCl_2$, $HgCl_2$, $MgCl_2$, KCl and NaCl were purchased from Energy Chemical Co., Ltd. (Shanghai, China) and Bide Pharmatech Co., Ltd. (Shanghai, China). Cupric chloride ($CuCl_2$) was obtained from Aladdin Reagent Co., Ltd. (Shanghai, China). Dimethyl sulfoxide (DMSO), 2-(N-morpholino) ethanesulfonic acid (MES) and glycerol were purchased from J&K Scientific Co., Ltd. (Beijing, China). The DNA aptamer ($Apt_{Cu}$; sequence: 5'-GACGACCACGGTAAACGACGCTGTACGGAGTGGTCTGTCGTC-3') was synthesized and HPLC-purified by Sangon Biotech Co., Ltd. (Shanghai, China). The working buffer (MES, pH 6.0) was prepared by dissolving 10 mM MES, 100 mM NaCl, and 5 mM $MgCl_2$ in ultrapure water.

## 1.2 Instruments

Fluorescence emission and UV–Vis absorption spectra were recorded using a TECAN Spark 10M multifunctional microplate reader. Fluorescence measurements were performed in 384-well black microplates with excitation at 416 nm and emission collected from 460 to 800 nm. Both excitation and emission slit widths were set to 20 nm. Circular dichroism (CD) spectra were acquired on a BioLogic MOS-450 spectrophotometer. Smartphone-based colorimetric analysis was conducted with a fixed smartphone mount positioned 15 cm above a 96-well transparent microplate under ambient and UV illumination (370 nm, 50 W). The NMR spectra were measured on a JNM-ECZL400S (400 MHz) spectrometer (JEOL, Japan). High-resolution mass spectrometry (HRMS) was performed using an ACQUITY UPLC-Class SYNAPT G2-Si HDMS system (Waters, USA). The pH values were determined using a FE28-Standard pH meter (Mettler-Toledo, Switzerland).

# 2. Methods

## 2.1 Fluorescence Binding Assay and $Cu^{2+}$ Detection

The DNA aptamer ($Apt_{Cu}$) was dissolved in ultrapure water to a final concentration of 100 μM. The aptamer solution was thermally annealed by heating it at 95 °C for 10 min, followed by gradual cooling to room temperature. RaC dyes were prepared by dissolving them in DMSO to create a 100 μM stock solution and stored in the dark at 4 °C.

RaC 10 was synthesized according to the previous report.[1-3] To investigate the interaction between RaC 10 and the aptamer, 10 μL of RaC 10 (100 μM) was mixed with 10 μL of $Apt_{Cu}$ (100 μM) in 180 μL MES buffer. Fluorescence spectra were recorded with emission intensities monitored at 495 nm and 665 nm. Data were collected using 384-well black microplates, with excitation and emission slit widths set to 20 nm. The samples were excited at 416 nm, and emission spectra were recorded from 460 to 800 nm. The binding constant ($K_d$) for the $Apt_{Cu}$-RaC 10 interaction was determined using the one-site binding model:[4]

$$F = F_0 + aK_d/(K_d + X)$$

where $X$ represents the concentration of the titrated analyte, $a$ is the maximum fluorescence change upon saturated binding.

To evaluate ratiometric fluorescence sensing performance, $Cu^{2+}$ at varying concentrations (0–50 μM) were added to the dye-aptamer mixture consisting of 10 μL RaC 10 (100 μM) and 14 μL $Apt_{Cu}$ (100 μM), diluted to 200 μL with MES buffer. All data are expressed as the mean of three independent experiments, with error bars indicating the standard deviation (SD).

**2.2 UV–Vis Absorption Assay**

For absorbance measurements, 10 μL of 100 μM RaC 10 was mixed with varying concentrations of $Apt_{Cu}$ in MES buffer, and the final volume was adjusted to 100 μL. The mixtures were transferred to a 96-well transparent microplate, and absorbance spectra were recorded from 300 to 850 nm using the Spark 10M reader.

**2.3 Smartphone-Based Colorimetric Detection**

For colorimetric analysis, sensor mixtures were transferred into a 96-well white microplate and photographed using a smartphone. The microplate was illuminated with UV light (370 nm), and the fluorescence color shift was visually observed. RGB values

from the images were extracted using the Color Picker App.

### 2.4 Circular Dichroism Spectroscopy

To assess the structural changes in the $Apt_{Cu}$ upon binding with RaC 10 and $Cu^{2+}$, circular dichroism (CD) spectra were recorded. Samples were prepared in MES buffer (10 mM MES, 100 mM NaCl, 5 mM $MgCl_2$, pH 6.0). Each sample (300 μL) was loaded into a 1 mm path-length quartz cuvette, and spectra were collected on a MOS-450 spectrophotometer from 220–400 nm with a bandwidth of 0.5 nm and a scan rate of 60 nm/min. Three scans were averaged for accuracy.

### 2.5 Real Sample Collection and Analytical Validation

Lake water samples were collected from the campus of Henan University of Technology and stored at 4 °C overnight to allow sedimentation. Prior to analysis, the samples were centrifuged at 5000 rpm for 10 min and subsequently filtered through 0.22 μm membrane filters to remove suspended particulates. Human biological samples, including serum, plasma, and urine, were obtained from the First Affiliated Hospital of Guangzhou Medical University and used in accordance with institutional guidelines. Prior to analysis, all real samples were diluted with the corresponding working buffer to minimize matrix effects, with dilution ratios of 1:5 for lake water, 1:10 for serum, 1:50 for plasma, and 1:10 for urine.

For $Cu^{2+}$ recovery experiments, the diluted samples were spiked with known concentrations of $Cu^{2+}$, followed by the addition of 10 μL RaC 10 (100 μM) and 14 μL $Apt_{Cu}$ (100 μM). The mixture was adjusted to a final volume of 200 μL using MES buffer to constitute the reaction system. The recovery efficiency and reproducibility of the RaCApt aptasensor were assessed in triplicate, demonstrating its applicability and reliability for $Cu^{2+}$ detection in complex environmental and biological samples.

## 3. Synthesis and Characterization

### 3.1 Synthesis of RaC 9

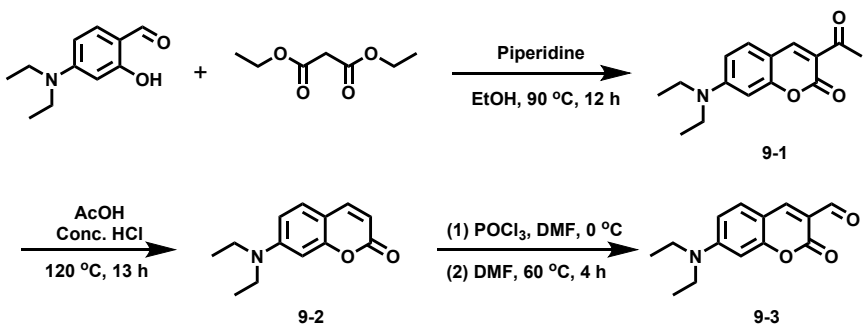


**Synthesis of compound 9-1**

4-(diethylamino)-2-hydroxybenzaldehyde (19 mmol, 3.67 g), diethyl malonate (38 mmol, 6.08 g) and piperidine (38 mmol, 3.23 g) were mixed with anhydrous ethanol (60 mL) and reacted by refluxing the mixture at 90 °C for 12 h. The reaction progression was detected by TLC. After the reaction was completed and cooled to room temperature, the reaction solution was rotary evaporated and the crude product **9-1** was freeze-dried and used directly in the next step without purification.

**Synthesis of compound 9-2**

Compound **9-1** (10 mmol, 2.59 g), acetic acid (20 mL) and concentrated hydrochloric acid (20 mL) were mixed and refluxed for 13 h at 120 °C. After cooling to room temperature, the reaction solution was poured into 100 mL of ice water. Then 40% NaOH solution was added dropwise to the reaction mixture to adjust the pH to 5.0. A precipitate was produced in the reaction mixture. And the crude product **9-2** (1.74 g, 80% yield) was obtained by filtering, washing four times with water and freeze-drying.

**Synthesis of compound 9-3**

Phosphorus oxychloride (29.7 mmol, 3.63 mL) was added dropwise to the DMF (29.7 mmol, 2.31 mL) at 0 °C under $N_2$ and stirred for 1 h. Then the DMF solution of compound **9-2** (10 mmol, 2.17 g) was added dropwise to the reaction solution and refluxed at 60 °C for another 4 h. Then the reaction solution was cooled to room temperature, added to 100 mL of ice water and stirred for 1 h. The filtered precipitates were washed twice with water and ether respectively to give an orange-yellow solid, which was freeze-dried to give compound **9-3** (1.85 g, 85% yield). $^1$H NMR (500 MHz, DMSO-$d_6$) δ 9.89 (s, 1H), 8.40 (s, 1H), 7.67 (d, $J$ = 9.1 Hz, 1H), 6.85 – 6.78 (m, 1H),

6.60 (d, $J$ = 2.2 Hz, 1H), 3.50 (q, $J$ = 7.0 Hz, 4H), 1.14 (t, $J$ = 7.0 Hz, 6H).

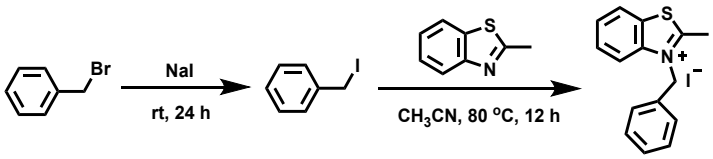


9-4 9-5

**Synthesis of compound 9-4**

Benzyl bromide (60 mmol, 10.27 g) was mixed with sodium iodide (120 mmol, 18 g) and acetone (80 mL), stirred at room temperature and protected from light for 24 h. Upon completion, the mixture was quenched by adding water (50 mL) and extracted with ether (200 mL). Then the organic phase was removed under reduced pressure to afford crude adduct. The crude product was purified by rapid column chromatography to obtain compound **9-4** (12.65 g, 97% yield). $^1$H NMR (400 MHz, $CDCl_3$) δ 7.45 – 7.40 (m, 2H), 7.37 – 7.27 (m, 3H), 4.49 (s, 2H).

**Synthesis of compound 9-5**

2-Methylbenzothiazole (16.9 mmol, 2.52 g), compound **9-4** (8.1 mmol, 1.77 g) and acetonitrile (5 mL) were mixed and refluxed at 80 °C for 12 h. After the reaction was completed, the reaction system was cooled to room temperature, and then the mixture was filtered. The filter residue obtained was washed with anhydrous ether three times and then subjected to vacuum drying, thereby obtaining compound **9-5**. $^1$H NMR (400 MHz, DMSO-$d_6$) δ 8.53 – 8.48 (m, 1H), 8.22 – 8.18 (m, 1H), 7.86 – 7.77 (m, 2H), 7.43 – 7.35 (m, 3H), 7.34 – 7.30 (m, 2H), 6.09 (s, 2H), 3.28 (s, 3H).

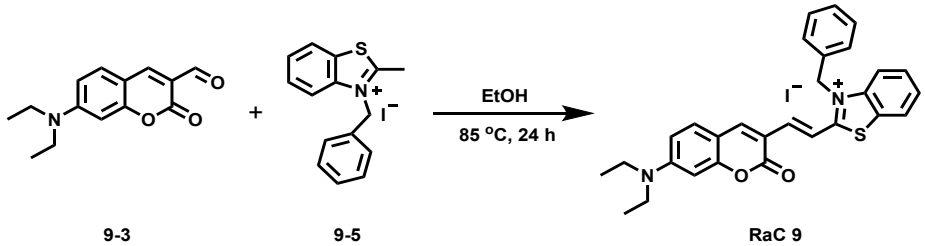


9-3 9-5 RaC 9

**Synthesis of compound RaC 9**

Compound **9-3** (0.56 mmol, 0.13 g), compound **9-5** (0.34 mmol, 0.13 g) and EtOH (2 mL) were mixed and refluxed at 85 °C for 24 h. After the reaction was completed, reaction system was cooled to room temperature, and then the mixture was filtered. The filter residue obtained was washed with cold ethanol three times and then subjected to

vacuum drying to obtain **RaC 9** (0.23 g, 70% yield). $^1$H NMR (500 MHz, DMSO-$d_6$) δ 8.59 (s, 1H), 8.42 (d, $J$ = 7.5 Hz, 1H), 8.21 (d, $J$ = 8.4 Hz, 1H), 8.13 (q, $J$ = 15.3 Hz, 2H), 7.82 – 7.78 (m, 1H), 7.77 – 7.72 (m, 1H), 7.57 (d, $J$ = 9.1 Hz, 1H), 7.42 – 7.38 (m, 2H), 7.37 – 7.32 (m, 3H), 6.88 (dd, $J$ = 9.1, 2.3 Hz, 1H), 6.67 (d, $J$ = 2.1 Hz, 1H), 6.07 (s, 2H), 3.54 (q, $J$ = 7.0 Hz, 4H), 1.16 (t, $J$ = 7.0 Hz, 6H). HRMS (ESI) m/z: calcd. for $C_{29}H_{27}N_2O_2S^+$ $[M]^+$ 467.1788; found 467.1814.

### 3.2 Synthesis of RaC 10

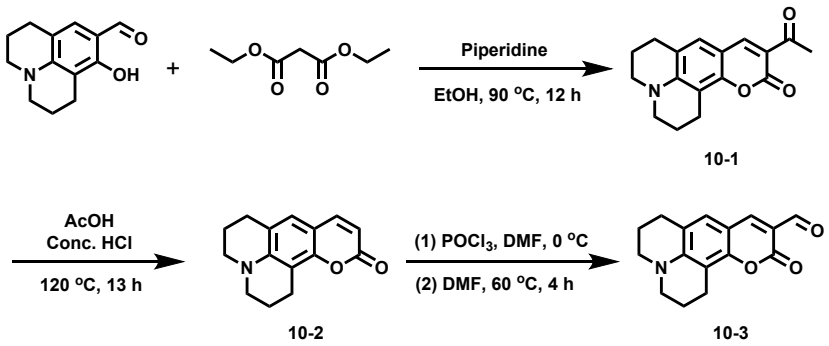


**Synthesis of compound 10-1**

Hydroxyjulonidine-9-formaldehyde (5 mmol, 1.08 g), diethyl malonate (10 mmol, 1.08 g), and piperidine (10 mmol, 0.85 g) were dissolved in ethanol (25 mL) and refluxed at 90 °C for 12 h. The reaction was detected by TLC. Upon completion of the reaction, cooled the system to ambient temperature. Then the solvent was removed to obtain adduct **10-1** and directly used in the next step without purification.

**Synthesis of compound 10-2**

A solution of compound **10-1** (4 mmol, 1.13 g) in 10 mL of acetic acid and concentrated hydrochloric acid (10 mL) were mixed and refluxed at 120 °C for 13 h. Upon completion of the reaction, the reaction mixture was cooled to ambient temperature and subsequently poured into 50 mL of ice water. Thereafter, a 40% aqueous NaOH solution was added dropwise to the reaction mixture to adjust the pH to 5.0. Upon the formation of a precipitate in the mixture, the precipitate was filtered off and rinsed with deionized water four times. Subsequently, the resulting mixture was subjected to lyophilization, yielding compound **10-2** (0.77 g, 80% yield). $^1$H NMR (500 MHz, DMSO-$d_6$) δ 7.72 (d, $J$ = 9.3 Hz, 1H), 7.01 (s, 1H), 5.92 (d, $J$ = 9.3 Hz, 1H), 3.27 – 3.22 (m, 4H), 2.74 – 2.68 (m, 4H), 1.90 – 1.83 (m, 4H).

**Synthesis of compound 10-3**

Phosphorus oxychloride (9 mmol, 1.21 mL) was added dropwise to the DMF (9 mmol, 0.70 mL) at 0 °C under an $N_2$ atmosphere. Compound **10-2** (3 mmol, 0.72 g) was first dissolved in 4 mL of DMF, and the resulting solution was added dropwise to above solution. The reaction mixture was then refluxed at 60 ℃ for a duration of 4 h. Upon cooling to ambient temperature, the reaction solution was added dropwise into 50 mL of ice water, and the resulting mixture was stirred continuously for 1 h. After a brown solid precipitated, the crude product was filtered out, then washed twice with water and diethyl ether respectively, and finally lyophilized to obtain compound **10-3** (0.73 g, 92% yield). $^1$H NMR (500 MHz, DMSO-$d_6$) δ 9.87 (s, 1H), 8.25 (s, 1H), 7.26 (s, 1H), 3.39 – 3.36 (m, 4H), 2.74 – 2.69 (m, 4H), 1.90 – 1.85 (m, 4H).

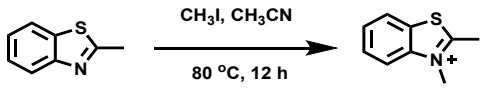


10-4

**Synthesis of compound 10-4**

2-Methylbenzothiazole (16.9 mmol, 2.52 g) and iodomethane (8.1 mmol, 1.15 g) were dissolved in 5 mL of acetonitrile and refluxed at 80 ° C for 12 h. After the reaction was completed, the reaction mixture was cooled to room temperature. The resulting precipitate was then washed with diethyl ether and freeze-dried to obtain white solid product **10-4** (1.9 g, 85% yield). $^1$H NMR (500 MHz, DMSO-$d_6$) δ 8.39 (d, $J$ = 8.1 Hz, 1H), 8.26 (d, $J$ = 8.5 Hz, 1H), 7.91 – 7.86 (m, 1H), 7.82 – 7.77 (m, 1H), 4.17 (s, 3H), 3.14 (s, 3H).

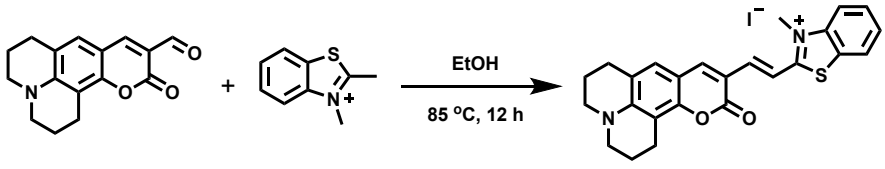


10-3 10-4 RaC 10

**Synthesis of compound RaC 10**

Compound **10-3** (0.40 mmol, 0.11 g) and compound **10-4** (0.40 mmol, 0.12 g) were dissolved in 10 mL of ethanol, and the mixture was refluxed for 12 h. Upon completion, the solvent was removed under reduced pressure. And crude mixture obtained was

purified by silica gel column chromatography (DCM: EtOH = 100:1) to afford product **RaC 10** (0.10 g, 60% yield). $^{1}$H NMR (500 MHz, DMSO-$d_6$) δ 8.46 (s, 1H), 8.34 (d, $J$ = 8.7 Hz, 1H), 8.18 (d, $J$ = 8.5 Hz, 1H), 8.05 – 7.92 (m, 2H), 7.87 – 7.78 (m, 1H), 7.77 – 7.68 (m, 1H), 7.16 (s, 1H), 4.19 (s, 3H), 3.45 – 3.35 (m, 4H), 2.80 – 2.70 (m, 4H), 1.70 – 1.82 (m, 4H). $^{13}$C NMR (101 MHz, DMSO-$d_6$) δ 171.4, 159.6, 151.9, 149.3, 147.8, 144.8, 141.9, 129.1, 127.8, 127.3, 123.9, 120.4, 116.2, 110.4, 109.9, 108.8, 105.2, 50.30, 49.9, 49.3, 35.7, 26.6, 20.4, 19.4, 19.3. HRMS (ESI) m/z: calcd. for $C_{25}H_{23}N_2O_2S^+$ $[M]^+$ 415.1475; found 415.1488.

### 3.3 Synthesis of ThT-π-NM

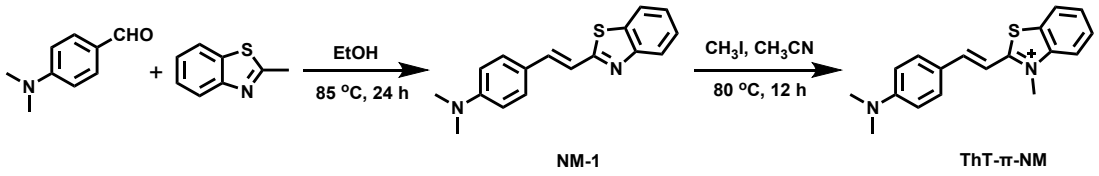


**Synthesis of compound NM-1**

*p*-Dimethylaminobenzaldehyde (10.0 mmol, 1.49 g) and 2-methylbenzothiazole (15.0 mmol, 2.24 g) were added to ethanol (50 mL) and refluxed for 24 h. Upon completion of the reaction, the system was cooled to room temperature, followed by filtration of the mixture. The obtained crude product was washed with cold ethanol to remove impurities, and then dried under vacuum to yield a dark red solid **NM-1** which could be used directly in the next step without purification.

**Synthesis of compound ThT-π-NM**

**NM-1** (5.0 mmol, 1.40 g) and iodomethane (100.0 mmol, 14.19 g) were dissolved in 50 mL of acetonitrile, and the reaction was carried out at 85 °C for 12 h. Then the solvent was removed under reduced pressure, and the resulting residue was purified by silica gel column chromatography to obtained dark red solid **ThT-π-NM** (1.14 g, 54% yield). $^{1}$H NMR (500 MHz, DMSO-$d_6$) δ 8.30 (d, $J$ = 8.0 Hz, 1H), 8.12 – 8.03 (m, 2H), 7.91 (d, $J$ = 8.8 Hz, 2H), 7.78 (t, $J$ = 7.8 Hz, 1H), 7.68 (t, $J$ = 7.8 Hz, 1H), 7.65 – 7.58 (m, 1H), 6.83 (d, $J$ = 8.9 Hz, 2H), 4.22 (s, 3H), 3.10 (s, 6H). $^{13}$C NMR (101 MHz, DMSO-$d_6$) δ 171.3, 153.5, 150.1, 141.9, 132.8, 128.8, 127.4, 126.8, 123.8, 121.4, 115.9,

111.9, 106.2, 39.7, 35.6. HRMS (ESI) m/z: calcd. for $C_{18}H_{19}N_2S^+$ $[M]^+$ 295.1264; found 295.1275.

# 4. Supplementary Figures and Tables

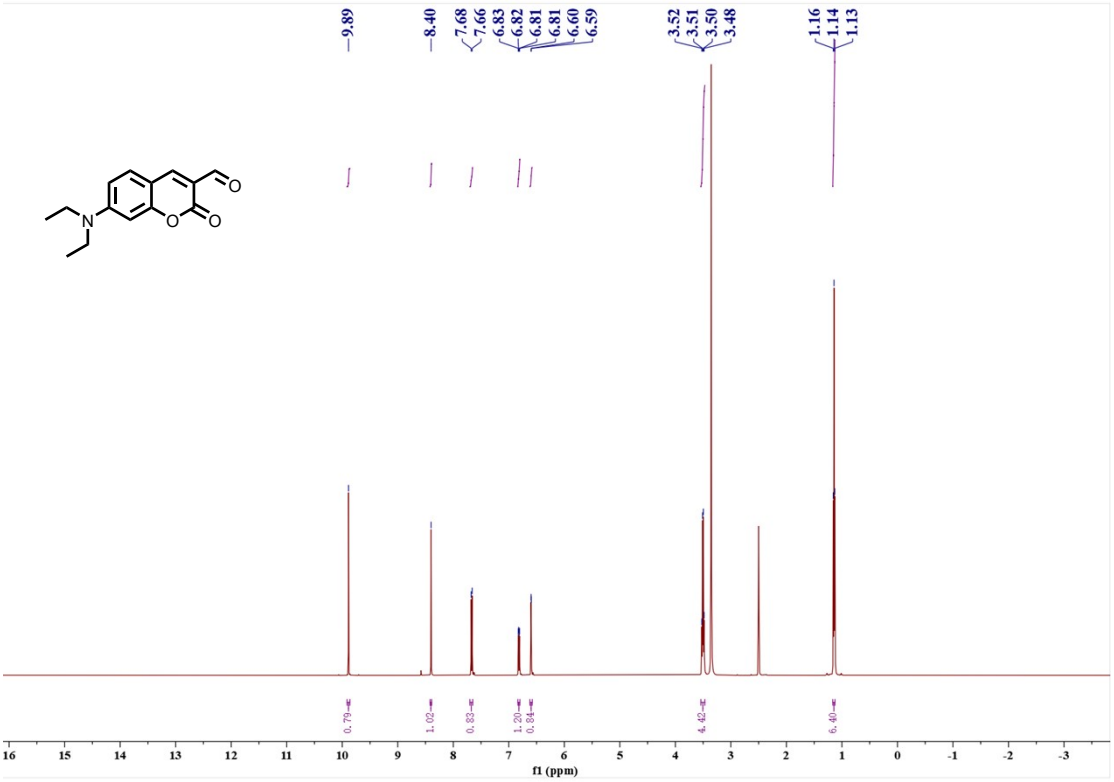


**Fig. S1** $^{1}$H NMR spectrum of compound **9-3** in DMSO-$d_6$.

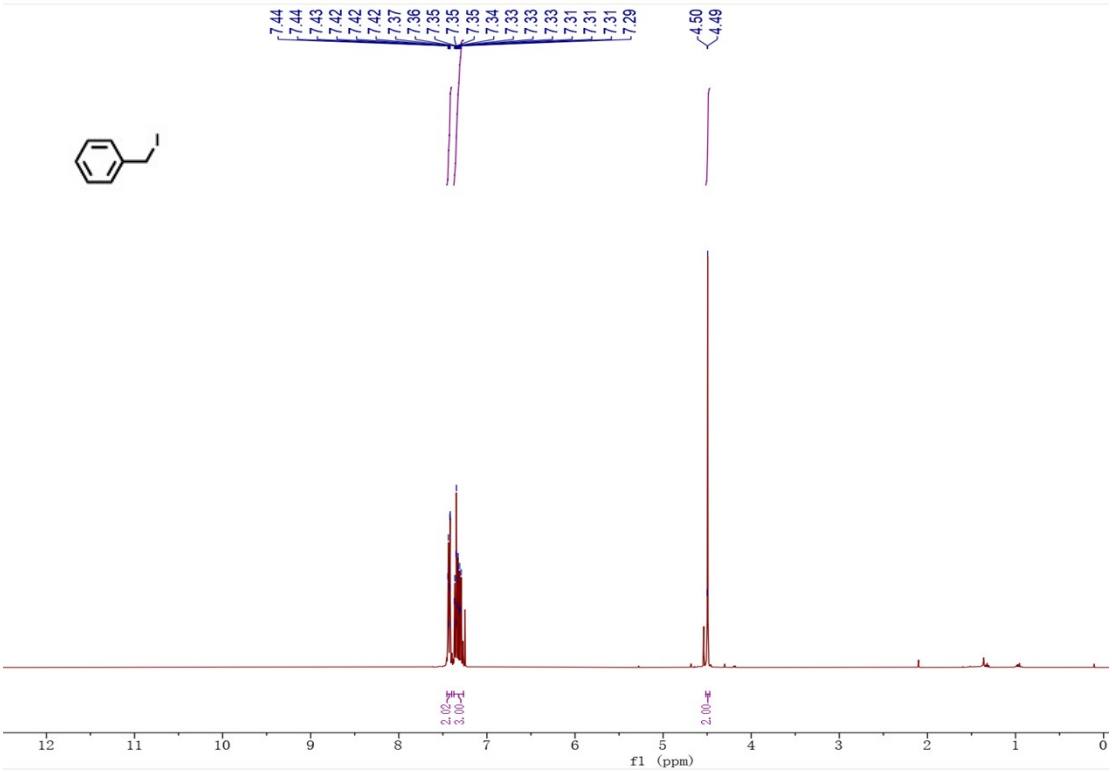


**Fig. S2** $^{1}$H NMR spectrum of compound **9-4** in $CDCl_3$.

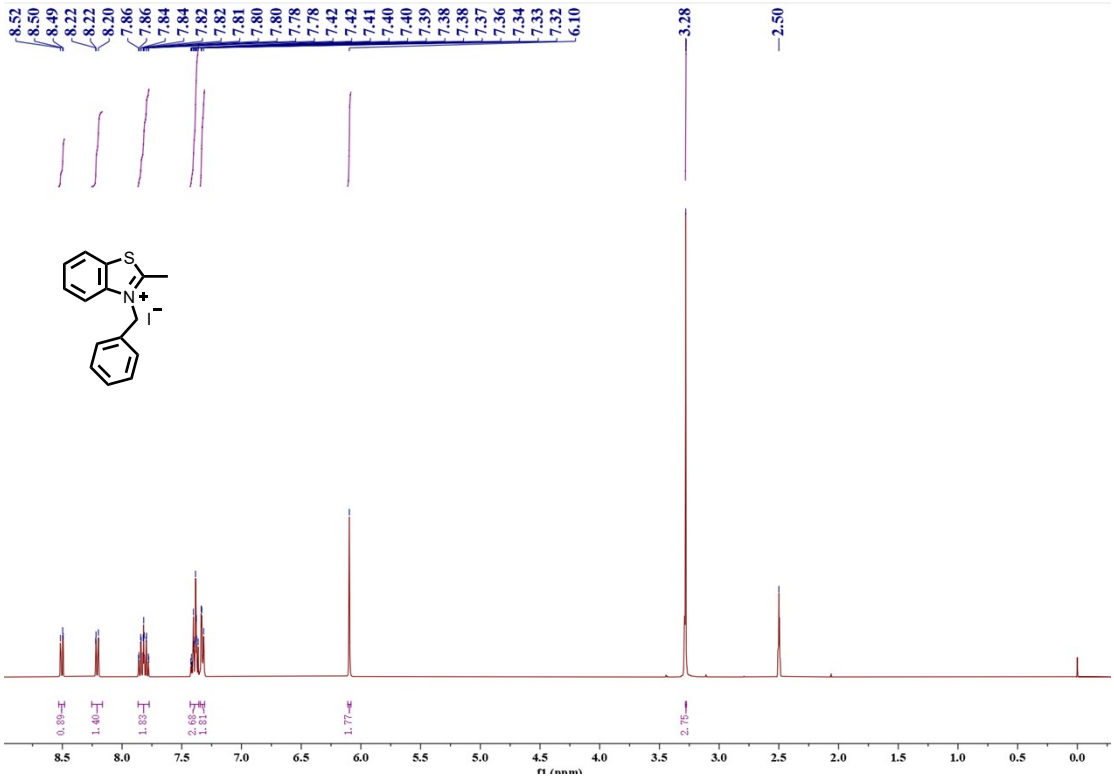

**Fig. S3** $^{1}$H NMR spectrum of compound **9-5** in DMSO-$d_6$.

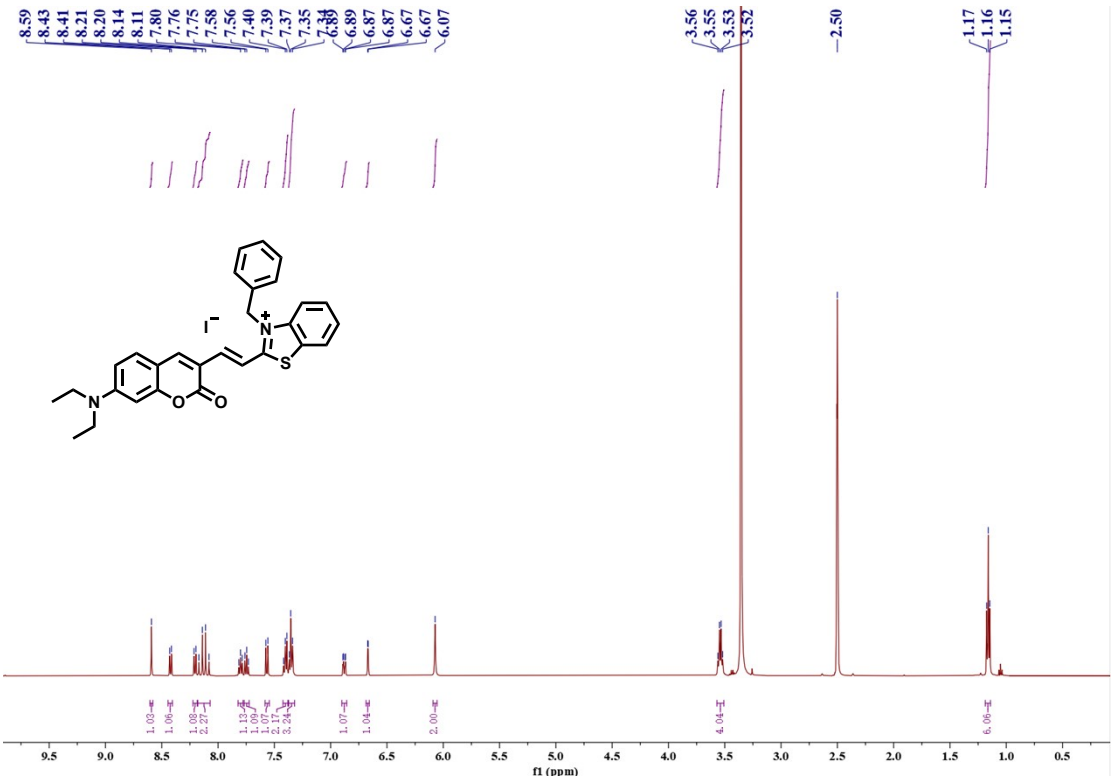

**Fig. S4** $^{1}$H NMR spectrum of **RaC 9** in DMSO-$d_6$.


**Fig. S5** $^{1}$H NMR spectrum of compound **10-2** in DMSO-$d_6$.

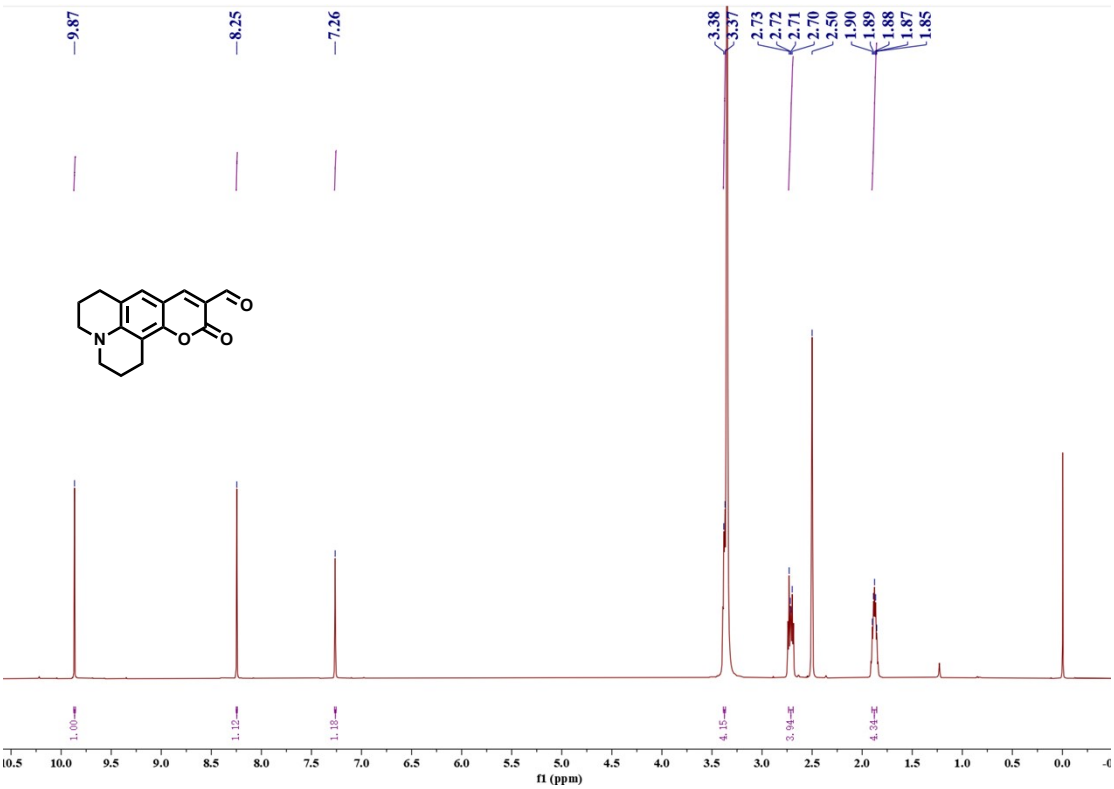


**Fig. S6** $^{1}$H NMR spectrum of compound **10-3** in DMSO-$d_6$.

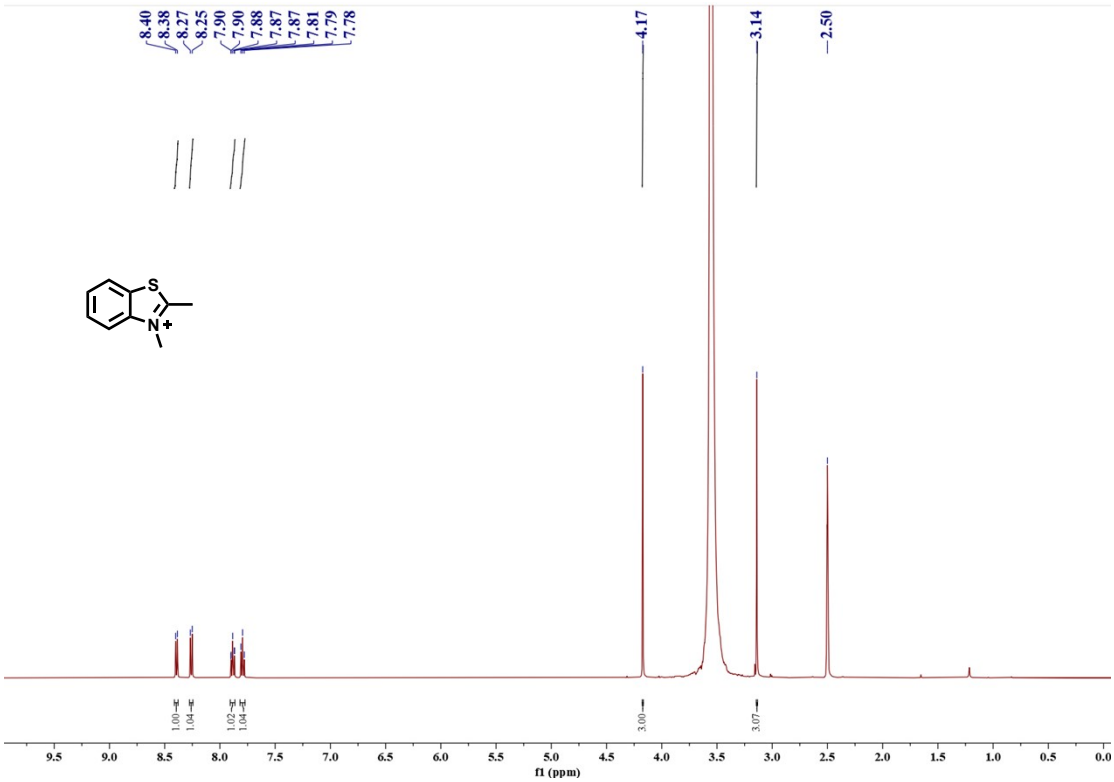


**Fig. S7** $^1$H NMR spectrum of compound **10-4** in DMSO-$d_6$.

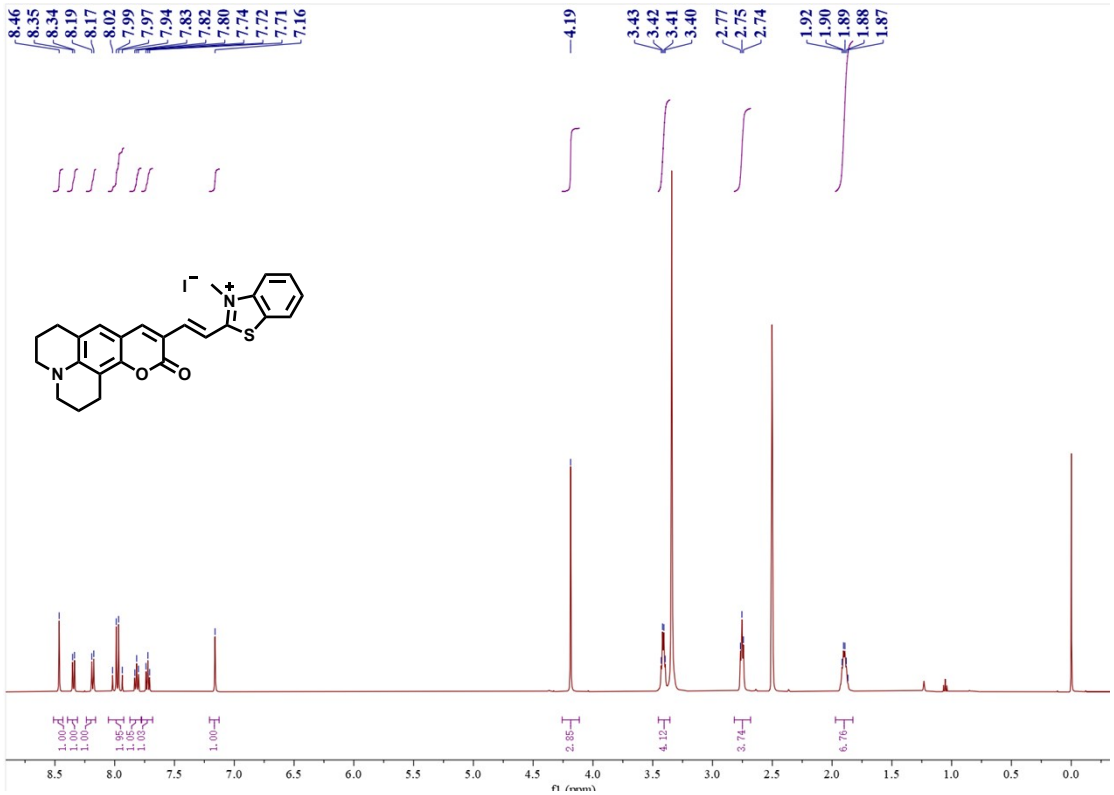


**Fig. S8** $^1$H NMR spectrum of **RaC 10** in DMSO-$d_6$.

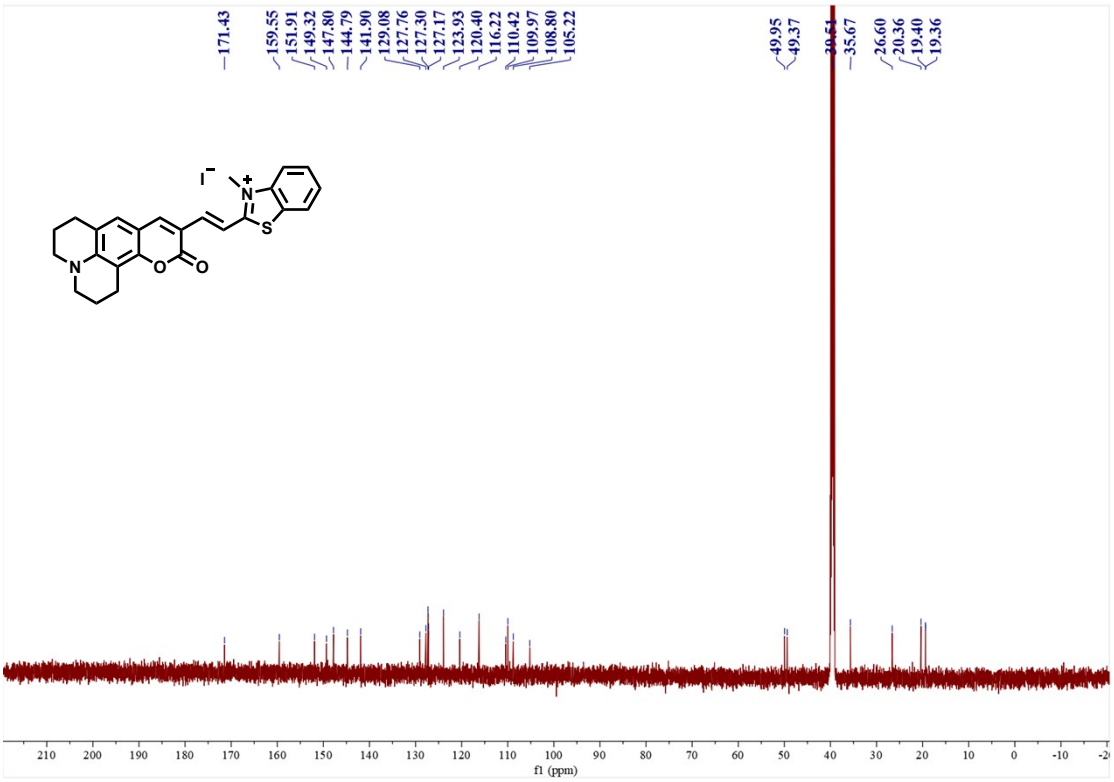


**Fig. S9** $^{13}$C NMR spectrum of **RaC 10** in DMSO-$d_6$.

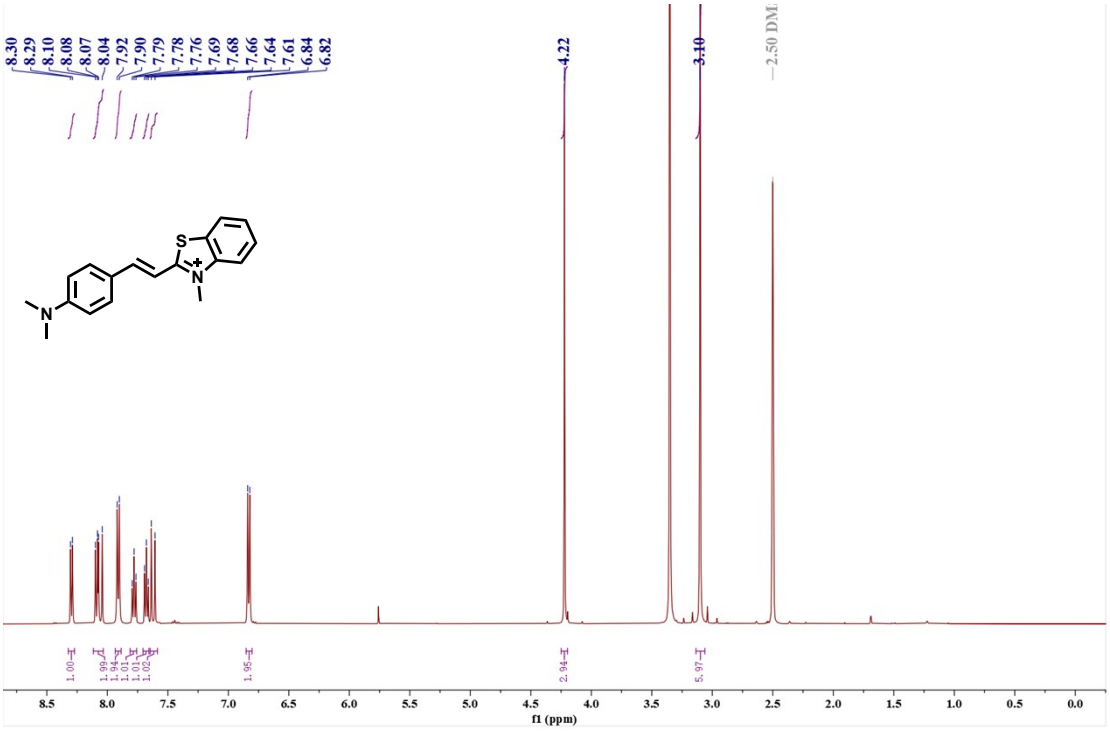


**Fig. S10** $^{1}$H NMR spectrum of **ThT-π-NM** in DMSO-$d_6$.

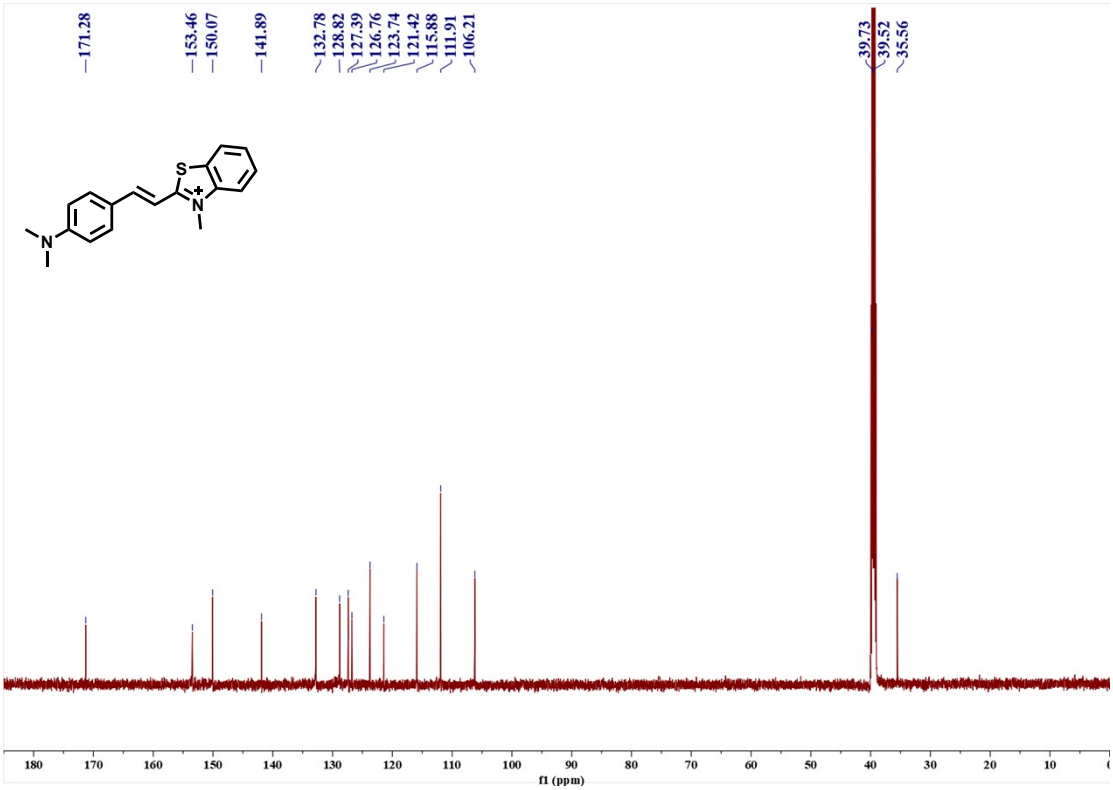


**Fig. S11** $^{13}$C NMR spectrum of **ThT-π-NM** in DMSO-$d_6$.

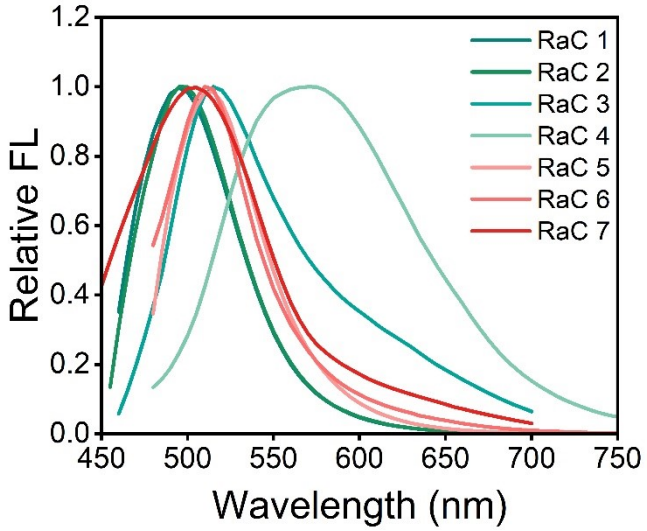


**Fig. S12** Fluorescence spectra of RaC 1 to RaC 7.

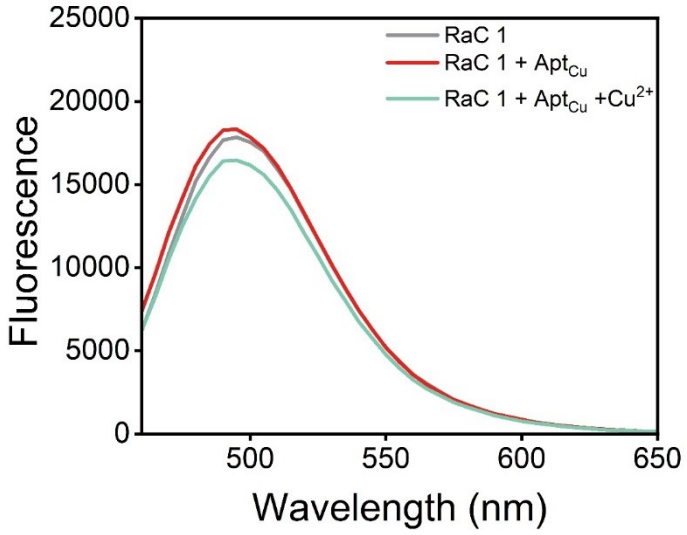


**Fig. S13** Fluorescence spectra of RaC 1 in the absence and presence of $Cu^{2+}$ (RaC 1, 5 μM; $Apt_{Cu}$, 4 μM; $Cu^{2+}$, 5 μM).

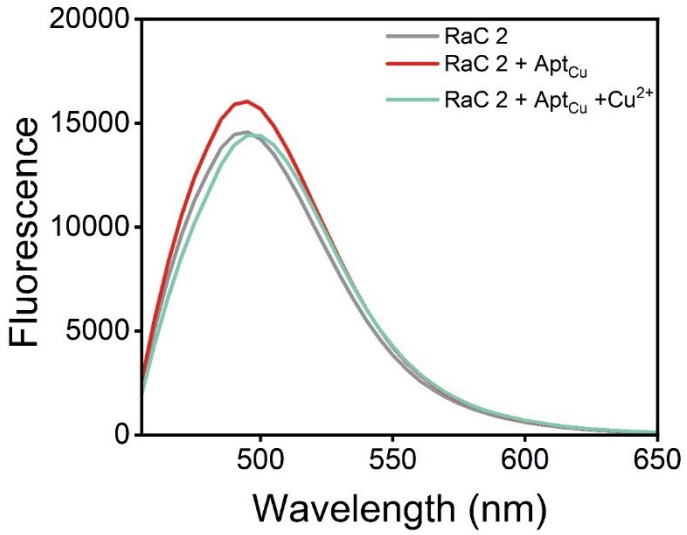


**Fig. S14** Fluorescence spectra of RaC 2 in the absence and presence of $Cu^{2+}$ (RaC 2, 5 μM; $Apt_{Cu}$, 4 μM; $Cu^{2+}$, 5 μM).

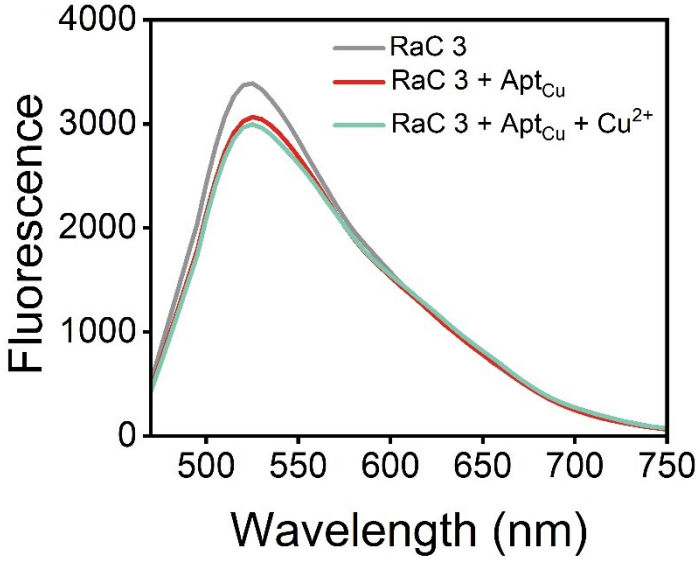


**Fig. S15** Fluorescence spectra of RaC 3 in the absence and presence of $Cu^{2+}$ (RaC 3, 5 μM; $Apt_{Cu}$, 4 μM; $Cu^{2+}$, 5 μM).

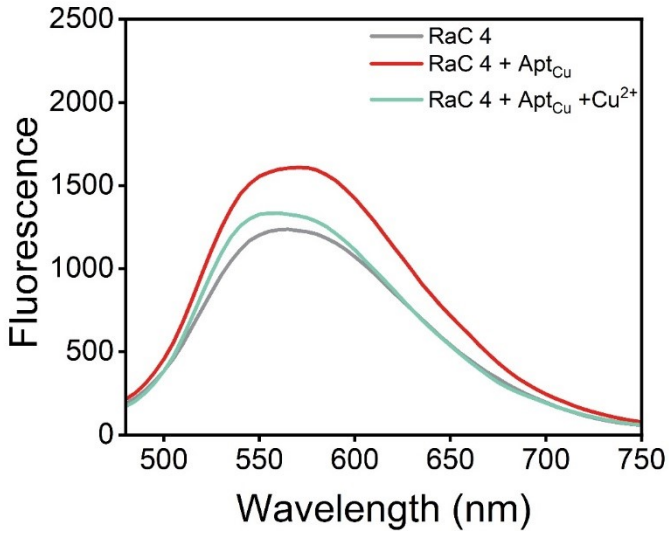


**Fig. S16** Fluorescence spectra of RaC 4 in the absence and presence of $Cu^{2+}$ (RaC 4, 5 μM; $Apt_{Cu}$, 4 μM; $Cu^{2+}$, 5 μM).

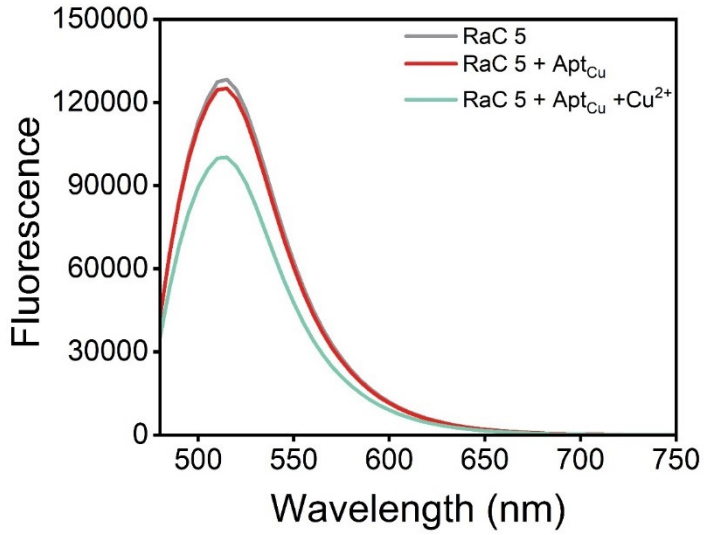


**Fig. S17** Fluorescence spectra of RaC 5 in the absence and presence of $Cu^{2+}$ (RaC 5, 5 μM; $Apt_{Cu}$, 4 μM; $Cu^{2+}$, 5 μM).

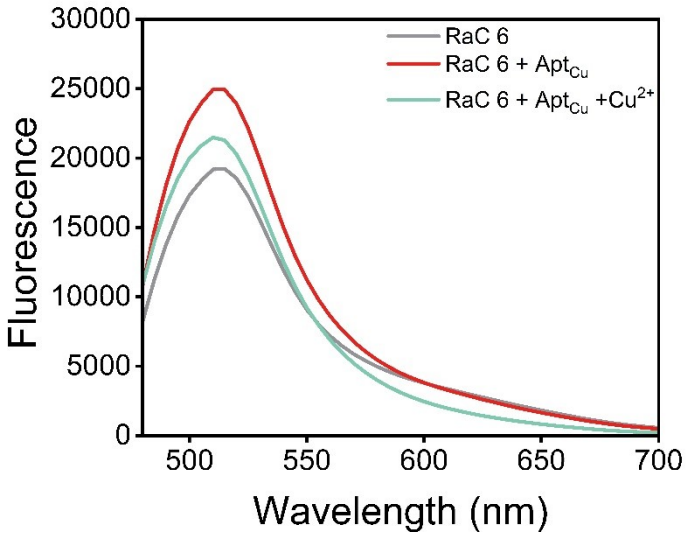


**Fig. S18** Fluorescence spectra of RaC 6 in the absence and presence of $Cu^{2+}$ (RaC 6, 5 μM; $Apt_{Cu}$, 4 μM; $Cu^{2+}$, 5 μM).

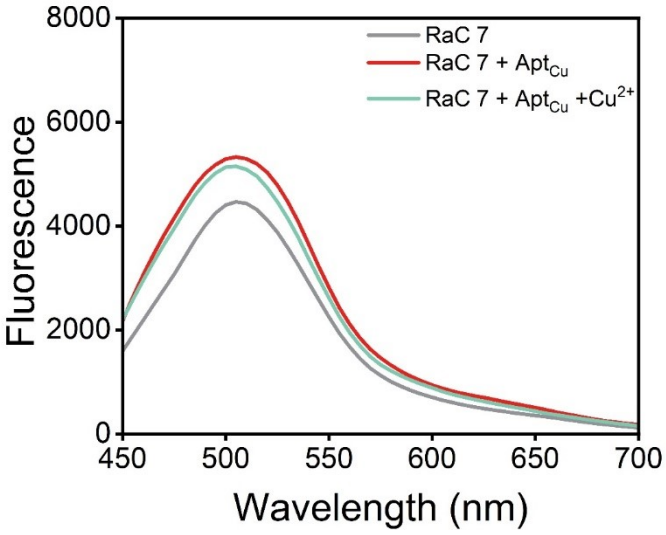


**Fig. S19** Fluorescence spectra of RaC 7 in the absence and presence of $Cu^{2+}$ (RaC 7, 5 μM; $Apt_{Cu}$, 4 μM; $Cu^{2+}$, 5 μM).

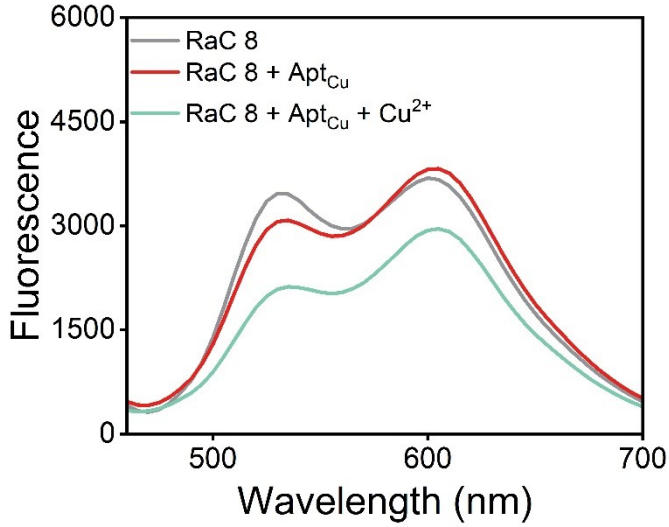


**Fig. S20** Fluorescence spectra of RaC 8 in the absence and presence of $Cu^{2+}$ (RaC 8, 5 μM; $Apt_{Cu}$, 4 μM; $Cu^{2+}$, 5 μM).

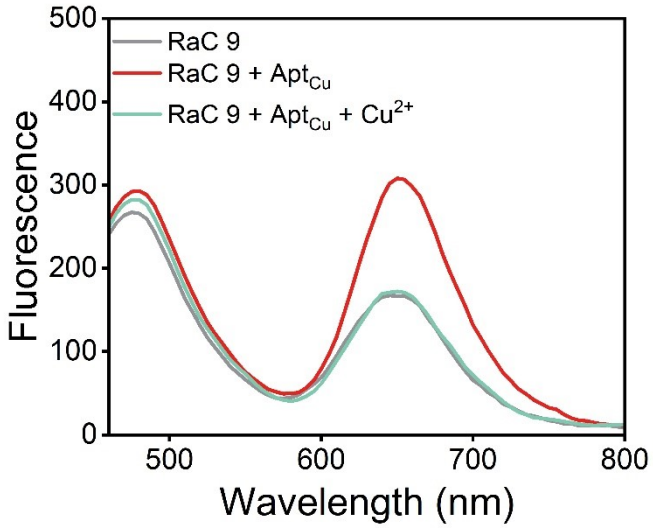


**Fig. S21** Fluorescence spectra of RaC 9 in the absence and presence of $Cu^{2+}$ (RaC 9, 5 μM; $Apt_{Cu}$, 4 μM; $Cu^{2+}$, 5 μM).

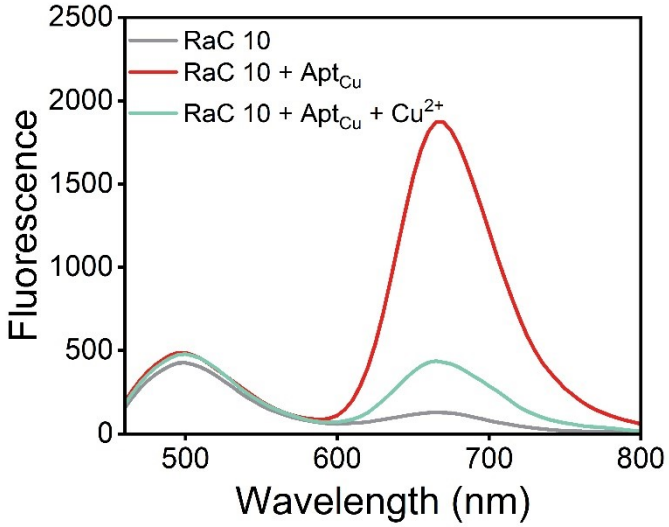


**Fig. S22** Fluorescence spectra of RaC 10 in the absence and presence of $Cu^{2+}$ (RaC 10, 5 μM; $Apt_{Cu}$, 4 μM; $Cu^{2+}$, 5 μM).

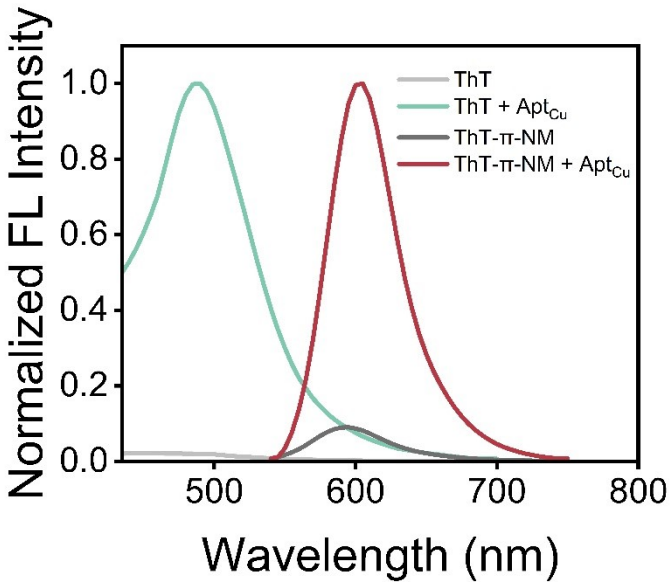


**Fig. S23** Fluorescence spectra of ThT and ThT-π-NM in the presence and absence of $Apt_{Cu}$.

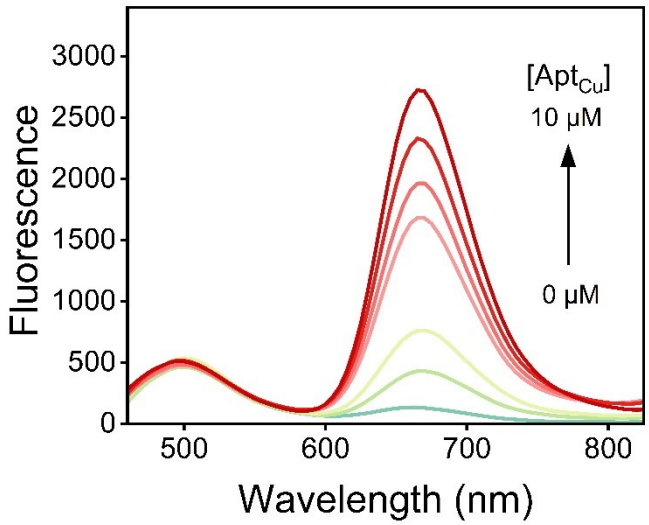


**Fig. S24** Fluorescence spectra of RaC 10 (5 μM) with increasing $Apt_{Cu}$ concentrations (0–10 μM), $\lambda_{ex}$ = 416 nm.

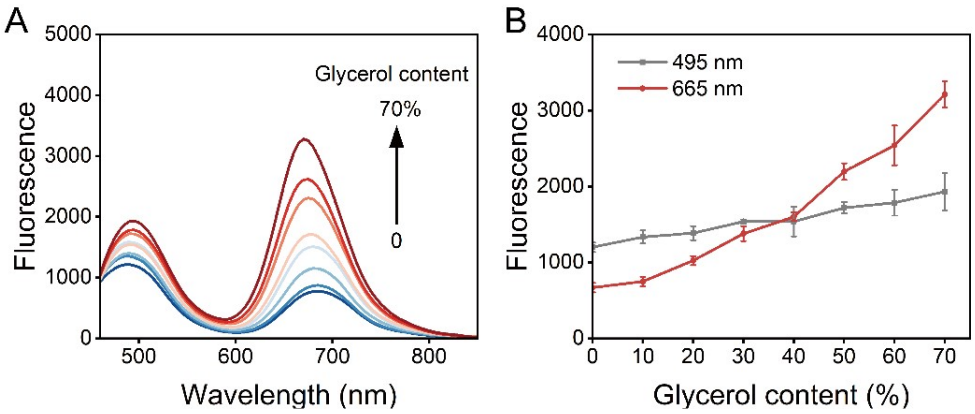


**Fig. S25** (A) Fluorescence spectra and (B) Fluorescence intensity changes of RaC 10 in glycerol/ethylene glycol mixtures.

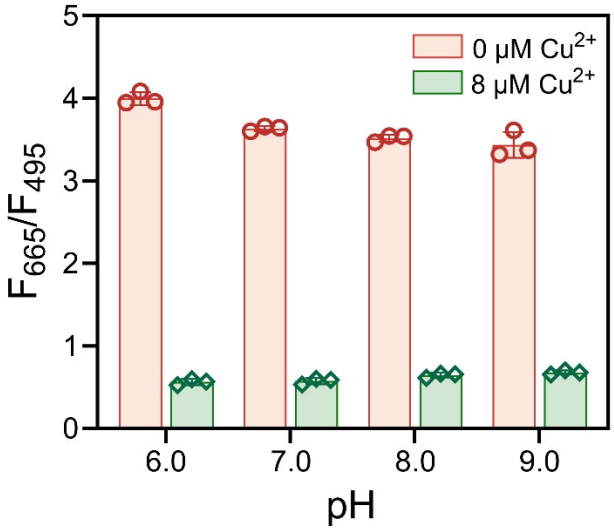


**Fig. S26** Effect of pH on the fluorescence response for $Cu^{2+}$ detection.

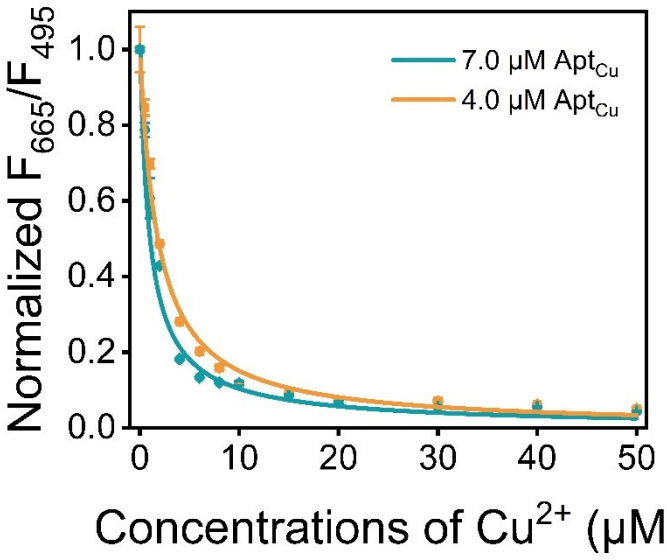


**Fig. S27** Fluorescence responses for $Cu^{2+}$ detection at varying $Apt_{Cu}$:RaC 10 molar ratios (0.8:1 and 1.4:1).

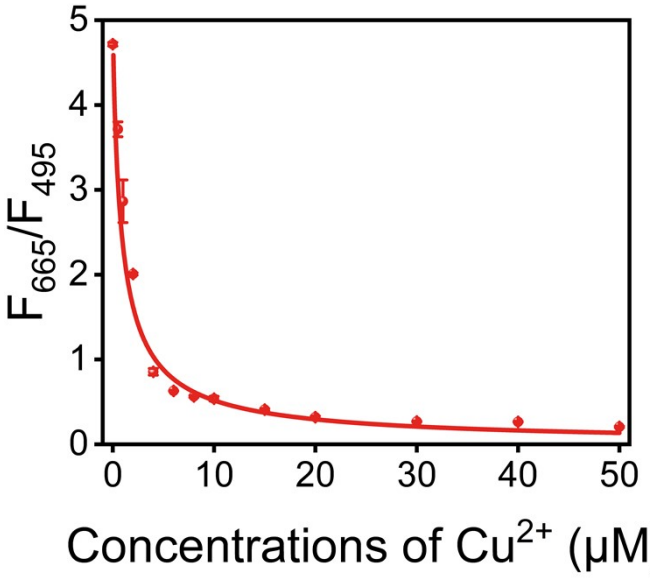


**Fig. S28** Fluorescence intensity of the RaCApt sensor upon addition of $Cu^{2+}$.

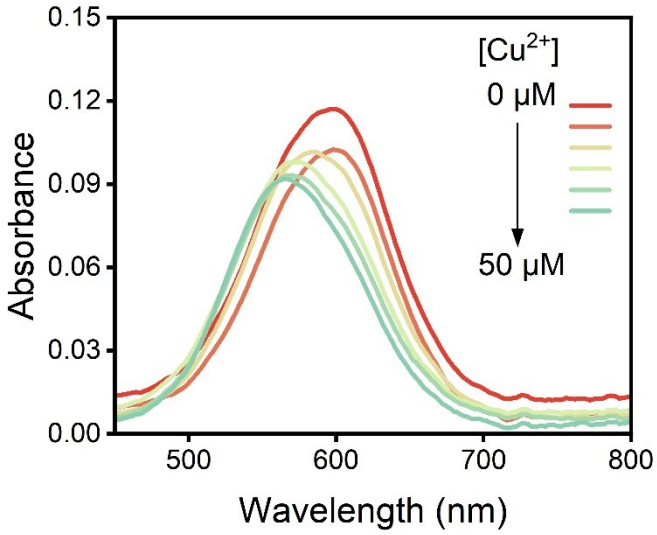


**Fig. S29** UV–Vis absorption spectra of the RaCApt sensor with varying $Cu^{2+}$ concentrations.

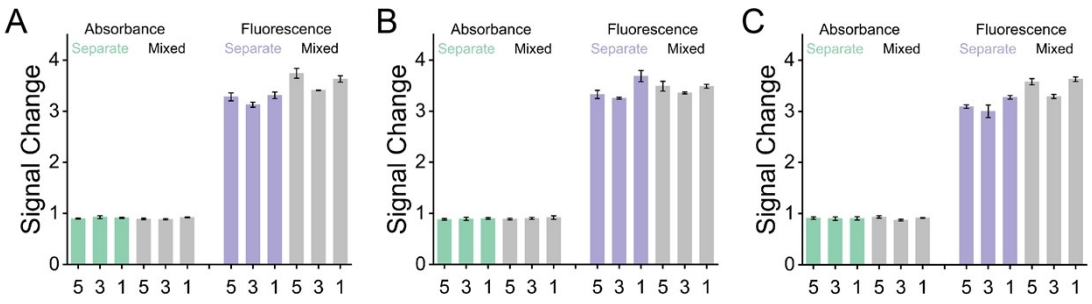


**Fig. S30** Storage stability of RaC 10, $Apt_{Cu}$, and the RaC 10/$Apt_{Cu}$ complex for $Cu^{2+}$ sensing after storage -20 °C, 4 °C, and 25 °C for 1, 3 and 5 days. In the "separate" mode, RaC 10 and $Apt_{Cu}$ were stored independently and mixed before testing; In the "mixed" mode, the pre-formed complex was stored prior to measurement.

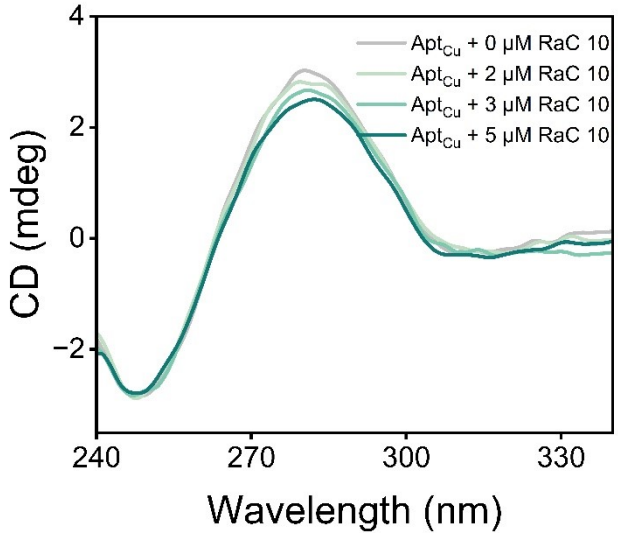


**Fig. S31** CD spectra after the addition of varying concentrations of RaC 10 to $Apt_{Cu}$.

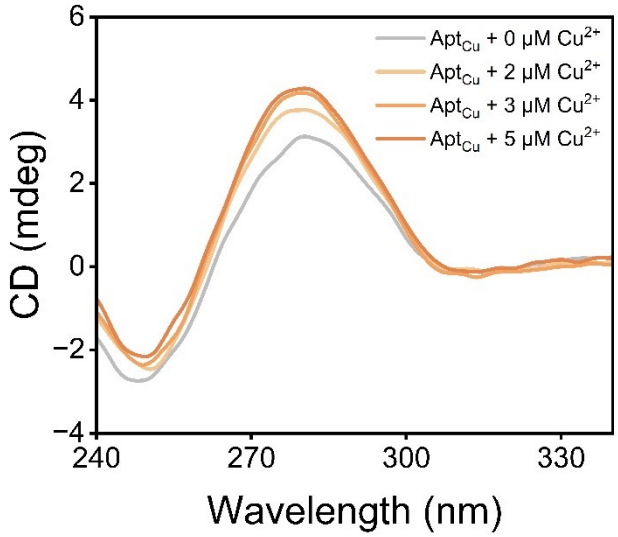


**Fig. S32** CD spectra after the addition of varying concentrations of $Cu^{2+}$ to $Apt_{Cu}$.

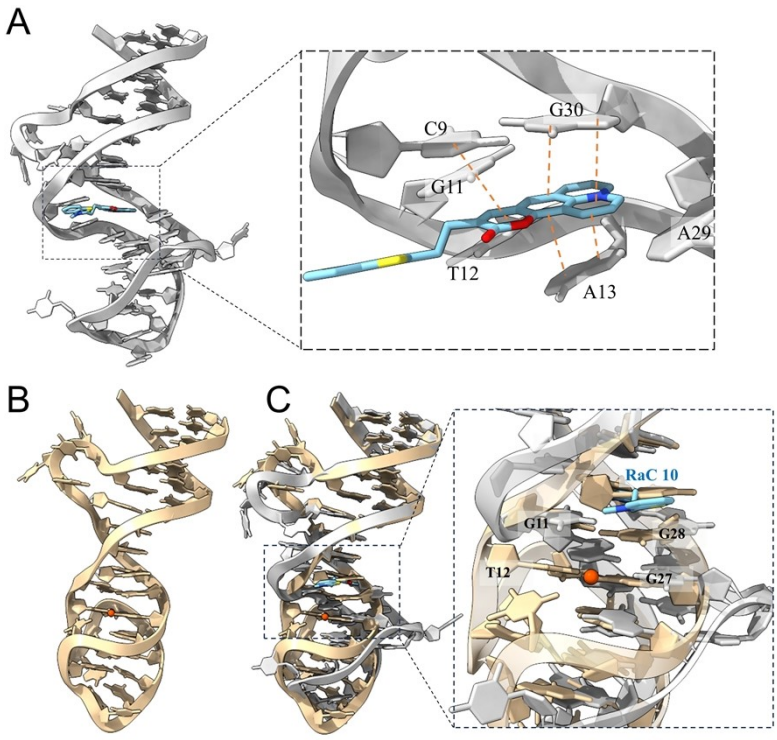


**Fig. S33** Predicted three-dimensional binding models of (A) RaC 10 and (B) $Cu^{2+}$ with $Apt_{Cu}$. (C) Spatial overlay of the $Cu^{2+}$- and RaC 10- binding sites within the $Apt_{Cu}$ structure.

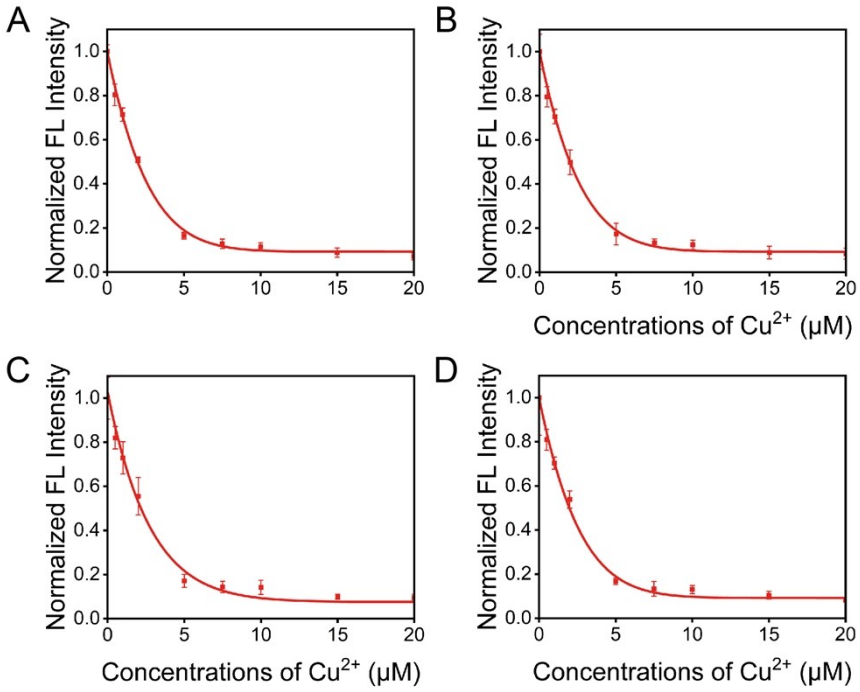


**Fig. S34** Fluorescence spectra of the RaCApt sensor in (A) lake water, (B) serum, (C) plasma, and (D) urine with varying $Cu^{2+}$ concentrations.

**Table S1** Comparison of representative $Cu^{2+}$ sensors and this work

| Recognition Mechanism | Signal modes | Linear range | LOD | Time | Refs |
|---|---|---|---|---|---|
| Conformational Switching & TICT | Ratiometric FL + Col | 0–4 μM | 0.183 μM | **5 s** | / |
| Chelation & LMCT | Solid-state Col | 0.047–1.57 μM | 3.15 nM | 1 min | 5 |
| ESIPT + ICT | Ratiometric FL + Col | 0–10 μM | 17 nM | 1 min | 6 |
| Static Quenching | FL + Col | FL: 0.1–50 μM<br>Col: 0.1–20 μM | FL: 5.61 nM<br>Col: 4.96 nM | 30 min | 7 |
| Competitive Displacement | NIR FL | 0–2 μM | 61 nM | 1 min | 8 |
| Electron Transfer | FL + Col | 5–400 μM | FL: 0.256 μM<br>Col: 0.225 μM | FL: 15 min<br>Col: 5 min | 9 |
| Ring Opening | FL | 0.16–1.4 μM | 40 nM | 1 min | 10 |

**Table S2** Determination of $Cu^{2+}$ in real samples

| Sample | Added (μM) | Found (μM) | Recovery (%) | RSD (%, n = 3) |
|---|---|---|---|---|
| Lake water | 0.5 | 0.472 | 94.40 | 1.57 |
| | 1.0 | 0.964 | 96.43 | 5.09 |
| | 2.0 | 2.068 | 103.42 | 6.39 |
| Serum | 0.5 | 0.467 | 93.53 | 5.39 |
| | 1.0 | 0.963 | 96.25 | 3.81 |
| | 2.0 | 2.114 | 105.70 | 6.49 |
| Plasma | 0.5 | 0.465 | 92.97 | 5.89 |
| | 1.0 | 0.954 | 95.44 | 8.46 |
| | 2.0 | 1.885 | 94.27 | 9.85 |
| Urine | 0.5 | 0.479 | 95.73 | 5.52 |
| | 1.0 | 1.056 | 105.64 | 3.24 |
| | 2.0 | 1.949 | 97.44 | 4.52 |

## References

1. G. Feng, X. Luo, X. Lu, S. Xie, L. Deng, W. Kang, F. He, J. Zhang, C. Lei and B. Lin, Angew. Chem., Int. Ed., 2019, 131, 6662-6666.

2. Z.-Y. Yu, W.-H. Luo, J.-E. Wang, H.-J. Diao, T.-Y. Wu, S.-T. Zeng, X.-C. Chen, Z.-S. Huang, J.-H. Tan and S.-B. Chen, Sens. Actuators, B, 2022, 361, 131730.

3. Y. Mou, Y. Zhang, M. Chen, X. Lin, J. Zhang, J. Han and X. Luo, Sens. Actuators, B, 2024, 408, 135529.

4. X. Li, Z. Yang, M. Waniss, X. Liu, X. Wang, Z. Xu, H. Lei and J. Liu, Anal. Chem., 2023, 95, 16366-16373.

5. A.P. Veedu, S.K. Kumar, S. Kuppusamy, A.M. Mohan, P. Deivasigamani, Surf. Interfaces, 2024, 48, 104301.

6. S.N.K. Elmas, F.N. Arslan, D. Aydin, Analyst., 2022, 12, 2687-2695.

7. J. Hou, P. Jia, K. Yang, T. Bu, S. Zhao, L. Li, L. Wang, ACS Appl. Mater. Interfaces, 2022, 14, 13848-13857.

8. J. Hu, X. Li, T.P. Loh, L.L. Bu, Anal. Methods, 2025, 17, 2536-2540.

9. M. Zhang, H. Yin, L. Wan, H. Gao, S. Liu, Y. Liu, Carbon Lett., 2024, 34, 1155-1164.

10. E.A. Namikuchi, R.D.L. Gaspar, I.M. Raimundo Jr, I.O. Mazali, Spectrochim. Acta A, 2024, 300, 122915.